Visible transmission response of nanoscale complementary metamaterials for sensing applications

2012 Nanotechnology 23 275503

(http://iopscience.iop.org/0957-4484/23/27/275503)

Nanotechnology **23** (2012) 275503 (6pp) doi:10.1088/0957-4484/23/27/275503

Visible transmission response of nanoscale complementary metamaterials for sensing applications

Zhe Liu[1], Xiaoxiang Xia[1], Yimin Sun[2], Haifang Yang[1], Rongyan Chen[1], Baoli Liu[1], Baogang Quan[1], Junjie Li[1] and Changzhi Gu[1]

[1] Beijing National Laboratory for Condensed Matter Physics, Institute of Physics, Chinese Academy of Sciences, Beijing 100190, People's Republic of China
[2] Delft University of Technology, PO Box 5046, 2600 GA Delft, The Netherlands

E-mail: jjli@iphy.ac.cn and czgu@iphy.ac.cn

Received 20 March 2012, in final form 15 May 2012
Published 18 June 2012
Online at stacks.iop.org/Nano/23/275503

Abstract
Metamaterials (MMs) have shown huge potential in sensing applications by detecting their optical properties, which can be designed to operate at frequencies from visible to mid-IR. Here we constructed complementary split ring resonator (CSRR) based metamaterials in nanoscale with unit length of 100 nm and slit width of 30 nm, and observed obvious responses in the visible waveband from 600 to 900 nm. These visible responses show a good tunability with the structure's geometry, and are well suited for dielectric detection. We demonstrated good refractive index sensing of CSRR based metamaterials in the visible region under both 0° and 90° polarized incidence. Our results extend the study of CSRR based metamaterials to the visible region, which is expected to deepen the understanding of the response mechanism of CSRRs and benefit their sensing applications in the visible region.

(Some figures may appear in colour only in the online journal)

1. Introduction

With the rapid development of nanofabrication processes on metamaterials (MMs) in recent years, a variety of plasmonic sensing devices is being designed for detection of biomolecules, H_2 gas or blood glucose concentration [1–4], which is valuable in our daily life. Plasmonic sensing using optical signals has particular advantages as it is label-free and non-invasive, and usually has a high sampling speed. Plasmonic sensing devices operate based on the surface plasmon, which is used to describe the collective electron oscillations triggered by impinging light on the metal surface. There are two types of surface plasmon for plasmonic sensing. One is propagating surface plasmon polaritons (SPPs), and related work was first demonstrated experimentally over two decades ago [5]. SPPs can be produced by grating coupling, hole array coupling and Kretschmann geometry [6–8], and the resonance frequency is closely related to the properties of the surrounding dielectric medium. The other one is the localized surface plasmon (LSP) which describes the coupling between the electromagnetic field and spatially confined free electrons. Since the resonance condition of the LSP is determined by the electron motions, its sensing performance can be optimized by alterations of the sizes and shapes of nanostructures. In this field, split ring resonator (SRR) based metamaterials have already been used in plasmonic sensing applications [4, 9–11], and the responses in related research have extended to the visible region [12].

Following the SRR based metamaterial structure, the complementary structure of SRR (CSRR) has been put forward based on the Babinet principle [13, 14]. Up to now, reported work on CSRR structures has been mainly focused in the microwave and terahertz regions [15–18], and few works have been carried out for CSRRs operating in the near-infrared and visible regions. Most importantly, the mechanism of the transmission property of a CSRR in the visible region is still ambiguous. The Babinet principle is suitable for a perfect metal in the microwave and terahertz regions, and can only

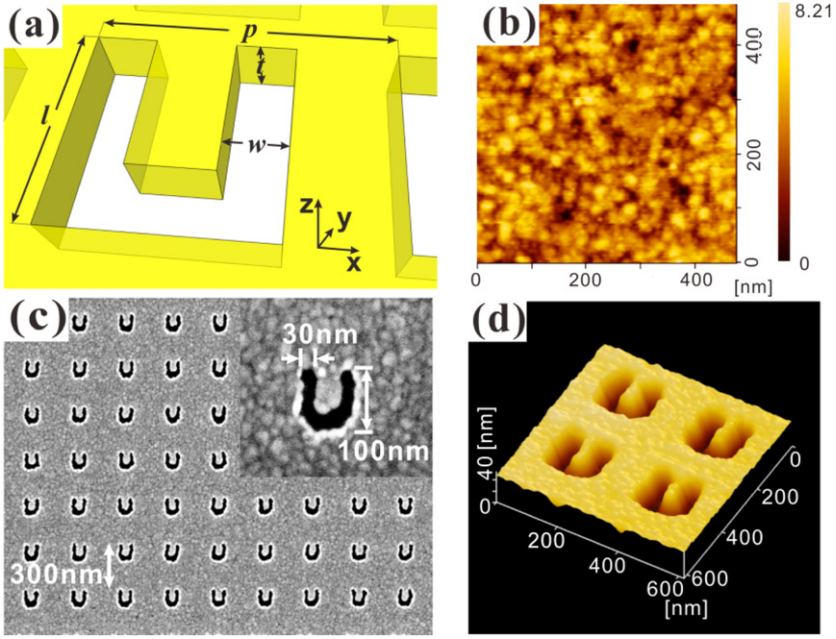

Figure 1. (a) Schematic view of a CSRR, with the parameters l, p, t, and w, which represent unit length, period, metal thickness and line width, respectively. (b) SPM image of the gold film with a thickness of 50 nm deposited by magnetron sputtering. (c) SEM image of a CSRR array with period $p = 300$ nm from the top view. The inset shows a typical CSRR unit with unit length $l = 100$ nm, line width $w = 30$ nm, and gold thickness $t = 50$ nm. (d) Three-dimensional SPM image of a four-unit structure with unit length $l = 200$ nm, period $p = 300$ nm, and gold thickness $t = 50$ nm.

qualitatively fit well at near-infrared optical frequencies [19]. The assumption of a perfect electric conductor for metals is not valid any more in the visible region, and the response of a subwavelength CSRR cannot be attributed to only the individual structure, but to collective responses. Moreover, CSRR MMs have the advantages that the large area of metal film can be an electrode to realize active modulation by applying external field on the sensing device, which benefits the optical sensing device and shows large potential for biomolecule detection [20].

In this work, nano-sized CSRR MMs were fabricated precisely by top-down nanofabrication technology, and their transmission properties and sensing properties were measured. From the optical transmission responses of the CSRRs, evident anisotropic visible responses in the waveband of 600–900 nm were observed, which showed a noticeable dependence on the array period, film thickness, unit geometry, as well as the incident polarization. The visible spectral resonances were regarded as the combination of SPP and waveguide modes (WMs), which can be used for refractive index (RI) sensing in the visible region. The results showed that the CSRRs had an RI sensitivity of about 210 nm/RIU. For different incident polarization, the resonance peaks shifted from 780 nm (830 nm) to 870 nm (935 nm) when the CSRRs were coated with BSA (bovine serum albumin). This work extends the study of CSRR MMs to the visible region and demonstrates an RI sensitive response of nanoscale CSRRs, which is helpful to deepen the understanding of the response mechanism of CSRRs and widen their applications in the visible region.

2. Sample fabrication and characterization

A schematic of the CSRR array and the coordinate system is shown in figure 1(a). The CSRRs were fabricated by electron-beam lithography and an ion-beam etching method. The top-down approach of ion-beam etching can avoid a large area lift-off process, and it has a high selection-ratio of the photoresist mask to gold film, which is very suited for precise fabrication of CSRR nanostructure. Gold films were deposited on quartz substrate (with a refractive index of about 1.46) by a magnetron sputtering method to obtain good roughness and small grain size, and the surface SPM image of the gold film with a thickness of 50 nm is shown in figure 1(b), from which the calculated corresponding root mean square (RMS) surface roughness of the film is ∼1.3 nm and the mean diameter of the grain is ∼15 nm. The large quantity of Au film benefits the following exposure and etching procedures. Figure 1(c) shows an SEM image of as-fabricated CSRR arrays with an array period of 300 nm, and an enlarged single unit of CSRR structure is inserted to show a fixed slit width of 30 nm and unit length of 100 nm. Figure 1(d) gives a three-dimensional SPM image of a four-unit structure with an array period of 300 nm and unit length of 200 nm, and it can be seen that the CSRR arrays have a good uniformity and sharp pattern profile. The geometrical parameters of the CSRRs are adjustable by controlling the fabrication process related parameters, for which the unit length of different samples ranges from 100 to 200 nm, the array period from 300 to 500 nm, and the thickness of gold films from 15 to 50 nm. Each sample is fabricated on a uniform area of 300 μm × 300 μm.

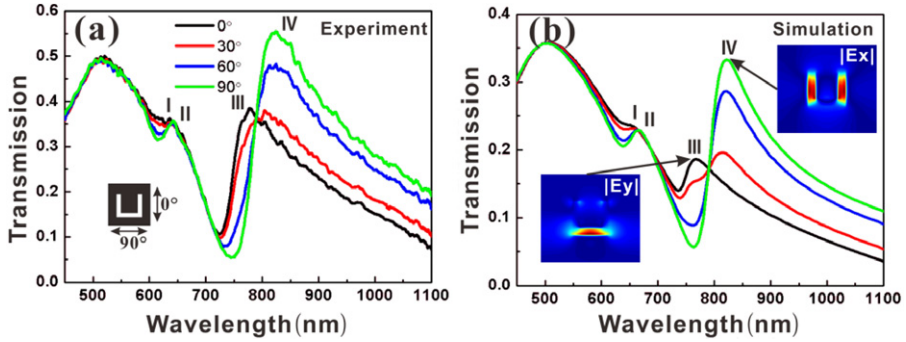

Figure 2. Transmission spectra of CSRRs by experiment (a) and simulation (b) under different polarized incident light conditions. The parameters of CSRR are $t = 30$ nm, $p = 400$ nm, $l = 150$ nm. The incident polarization is defined as the angle between the incident E field and the CSRR arms. The near-field electric field intensity distribution is simulated, corresponding to modes III and IV.

Optical measurements were carried out under different incident polarization angles θ from 0° to 90° to obtain the transmission spectra of the CSRR samples, where the polarization θ is defined as the angle between the incident E field and the y axis (along the CSRR arms). In addition, the finite-difference time-domain (FDTD) method was used to simulate the transmission spectra, electrical field intensity and phase distribution of the CSRR structures, using the freely available software package MEEP [21]. In the simulations, the Drude–Lorentz model was used to describe the dispersion of the gold, and the CSRR structure was placed on a semi-infinite quartz substrate with a refractive index of 1.46.

Typical normalized transmission spectra of a CSRR sample are shown in figure 2(a), the geometric parameters of which are listed as follows: metal thickness $t = 30$ nm, period $p = 400$ nm, and unit length $l = 150$ nm. The transmission spectra were obtained under four different incident polarization directions of $0°, 30°, 60°$ and $90°$. Figure 2(b) displays the results of the calculated transmission spectra for this CSRR sample, and it is easily seen that the calculated results are in good agreement with the experimental results shown in figure 2(a). The slight differences of peak intensity and position may originate from the deviation of the gold dispersion relation model used from that of real metal.

For all polarizations from 0° to 90° shown in figure 2(a), the transmission spectra show a fixed peak at a wavelength of 500 nm, which represents the interband transition of bound electrons from the 5d state to the 6sp state [22]. The contribution of interband transitions to the dielectric function $\varepsilon(\omega)$ is quite similar to that of the corresponding resonance in dielectric materials, which can be illustrated by $\varepsilon_{\text{Lorentz}}$. The bound electrons exert a huge influence on the transmission properties of gold in the visible region, and result in the constant 500 nm transmission peak. Since this 500 nm peak results from the nature of gold, we will not consider it in the following discussion. In addition, it can be seen from figures 2(a) and (b) that the transmission intensity of a certain polarization is a linear superposition of modes excited by orthogonal electric field components parallel to the x and y axes, respectively. Therefore we do not need to analyze the intermediate polarized mode but focus on the 0° and 90° incidence modes.

3. Physical origin of the resonances

Based on the experimental and simulated results, the physical origin of these resonance modes of nano-sized CSRRs was explored. Here, the origin of these resonances can be understood as a coupling effect of SPPs and WMs. With regard to one aspect, as periodic nanostructure arrays, SPPs are excited by the incident light on the interface between the dielectric and the metal in the form of

$$E_z^{\text{spp}} = -A\left(\frac{k_{\text{spp}}}{k_0\varepsilon_m}\right)\mathrm{e}^{-k_z z}\mathrm{e}^{\mathrm{i}k_{\text{spp}}x} \tag{1}$$

where $|\vec{k}_{\text{spp}}| = \omega/c[\varepsilon_m\varepsilon_{\text{d}}/(\varepsilon_m + \varepsilon_{\text{d}})]^{1/2}$; ε_{d} and ε_m are the permittivities of the dielectric and the metal, respectively [7, 23]. This reveals the SPPs' phase fluctuation on the xy-plane in (1). It is a kind of collective excitation of free electrons excited by incident electromagnetic (EM) waves. With regard to the other aspect, WMs also play a very important role in subwavelength grating and slit optical properties. The U-shaped CSRR structure can be divided into three slits, including two arms and a bridge connecting the two arms. Each slit allows an EM wave with electric field perpendicular to the slit to pass through as

$$|E^{\text{WM}}(z)\rangle = \sum_m |m\rangle[A_m\mathrm{e}^{\mathrm{i}q_{zm}z} + B_m\mathrm{e}^{-\mathrm{i}q_{zm}z}] \tag{2}$$

in which $|m\rangle$ denotes the mth mode, A_m and B_m are the expansion coefficients, and $q_{zm} = \sqrt{k_0^2 - (m\pi/w)^2}$ is the propagation constant of mode m for perfect metal [24]. However in real metal, the propagation constant should be replaced by a more complicated form [25]. These slits act as a waveguide which allows specific modes to pass through, and both the metal thickness t (in the z direction) and the line width w can change the WM phase. In this coupling mode for nano-sized CSRRs, the SPP and WMs are linked by their phase at the metal/dielectric interface.

Besides the polarizations of the incident light, the parameters of the CSRR structures including the structure period, metal thickness and unit length can also be used to modulate the transmission properties of the CSRR structure, which helps a lot in the exploration of related mechanisms. In the following, the influence of these size and shape related

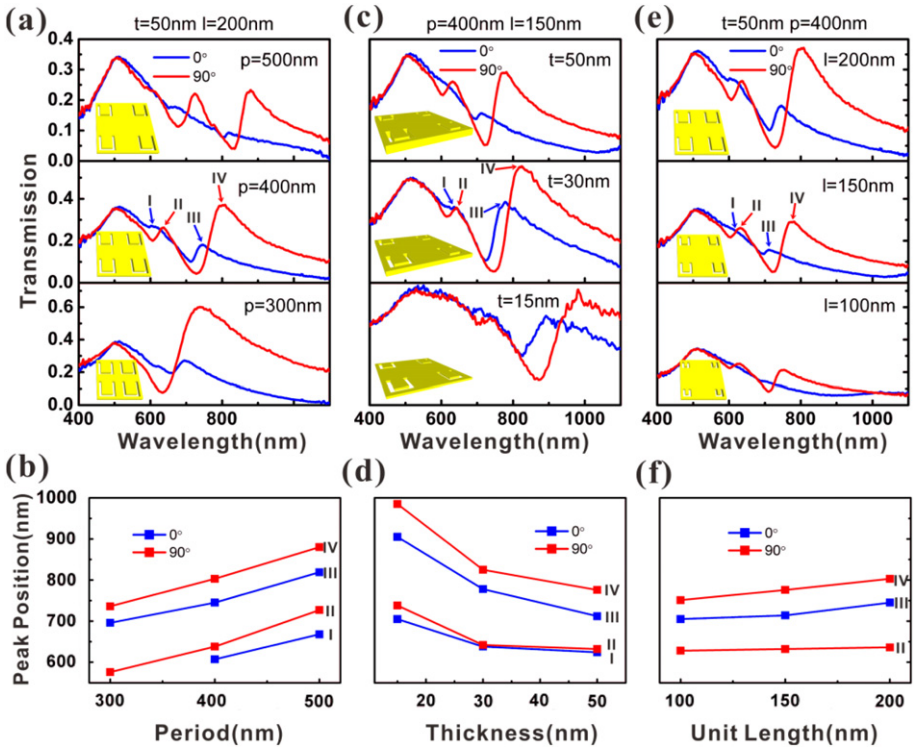

Figure 3. Transmission spectra of CSRRs with different parameters. (a) The period is varied from 300 to 500 nm with fixed $t = 50$ nm and $l = 200$ nm; (c) the metal thickness is varied from 15 to 50 nm with fixed $p = 400$ nm and $l = 150$ nm; (e) the unit length is varied from 100 to 200 nm with fixed $p = 400$ nm and $t = 50$ nm; (b), (d) and (f) show the response peak position as a function of period, metal thickness and unit length, respectively.

parameters will be systematically discussed. Figure 3(a) shows the results of measuring the transmission spectrum of a series of samples with fixed parameters $t = 50$ nm, $l = 200$ nm but varied period p from 300 to 500 nm. There were two resonance modes when p was 500 nm, which lie around 727 nm/880 nm under 90° polarized incidence, and 665 nm/822 nm under 0° polarized incidence. When p decreases, these modes have an obvious blue-shift, as shown in figure 3(b). The period dependent resonance shift mainly originates from change of the SPP modes. The incident wavevector can be changed by the reciprocal lattice vector $|\vec{G}_{x,y}| = 2\pi/p$. To obey the momentum matching condition, only the SPP wave with a wavevector $\vec{k}_{\rm spp} = \vec{k}_x \pm m\vec{G}_x \pm n\vec{G}_y$ can be excited. By increasing p, the $\vec{G}_{x,y}$ decreases followed by decrease of $|\vec{k}_{\rm spp}|$. The change of the SPP phase distribution will finally modify the transmission peak position.

Figure 3(c) shows the change of resonance peak with the thickness of gold film, where t is changed from 15 to 50 nm with fixed $l = 150$ nm and $p = 400$ nm. In figure 3(d), it is apparent that the resonance peak moves to a longer wavelength when the metal thickness decreases, for both 90° and 0° incident polarization. The phenomenon of thickness dependence should be attributed to the WMs. In figure 2(b), the simulated electric field intensity distributions were given for two resonance peaks. For mode III, the incidence polarization was 0°, and it led to *Ey* in the slit perpendicular to the polarization, which is the characteristic of a waveguide in a narrow slit. For mode IV, the opposite occurred, and the polarization of the excited modes in the two arms was still perpendicular to the slits. For the waveguide mode, the metal thickness t is an important factor. The phase of the propagation modes at the emitting side changes with variation of the metal thickness. The SPP and WMs are coupled at the emitting side of the metal layer, and the phase change alters the coupling of the SPP and the WMs. Thus, the increase of metal thickness can immensely change the WM phase and result in an obvious peak shift, which shows a tunable effect of the film thickness on the transmission responses.

In the following, we change the unit length of the CSRR arrays to observe its effect on the resonance peak. In figure 3(e), when l is changed from 100 to 200 nm, the resonance peak shift (figure 3(f)) is not as large as those when changing p and t. The peaks of mode I are not shown in figure 3(f) as they are hard to distinguish in figure 3(e). In the narrow slits, it is the short axis that has the greatest influence on the WM propagation in the visible range of interest, and not the long axis, so change of l causes a tiny peak shift. However, the existing peak shift comes from the length decrease of the slit, as the confinement of the resonant fields within the slit results in a decrease of peak wavelength [26]. These results indicate a tuning effect of the CSRR unit geometry on the transmission intensity and peaks.

Since the transmission resonance peaks shift slightly with change of unit length (figure 3(e)) but obviously with change of period (figure 3(a)), it is the SPP property which determines the appearance of different transmission peaks.

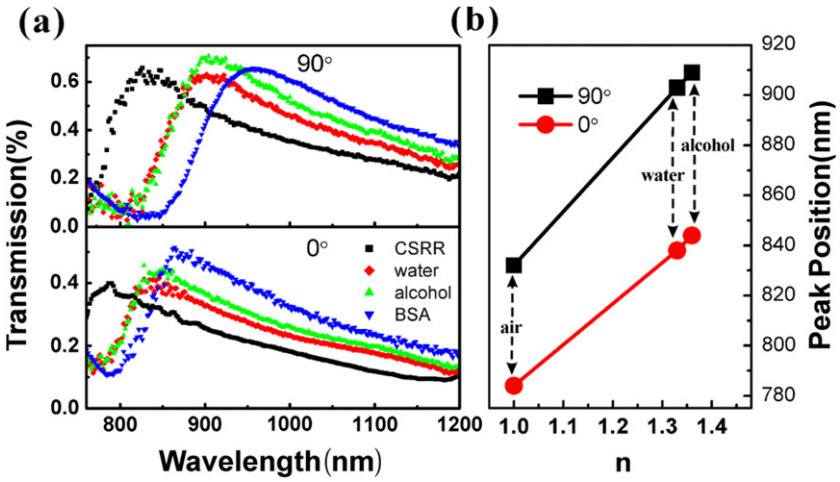

Figure 4. (a) Transmission spectra of CSRR coated by water, alcohol and BSA. (b) Resonance peak shift as a function of refractive index.

The two resonance peaks are mainly determined by the SPP momentum matching condition $\vec{k}_{\rm spp} = \vec{k}_x \pm m\vec{G}_x \pm n\vec{G}_y$, and can be modified by WMs in slits. The resonance peak with shorter wavelength disappears when p is 300 nm, as it is overlapped by the interband transmission peak at 500 nm.

4. Sensing application

Based on the discussion above, we concluded that the transmission property of a CSRR is closely related to both the array of structures (SPP determined) and the individual structure (WMs determined), and both of them are dielectric environment sensitive. For the SPP, the change of the dielectric constant $\varepsilon_{\rm d}$ on the CSRR can affect the wavevector $k_{\rm spp}$, and thus change the SPP mode in (1). For WMs, q_{zm} in (2) is closely related to $\varepsilon_{\rm d}$ and ε_m in real metal [25], and the $\varepsilon_{\rm d}$ can changes the phase of the WMs at the emission surface. Thus, RI sensing can be used on a CSRR for dielectric property detection. Here, the sensing sensitivity can be defined as $\mathrm{d}\lambda/\mathrm{d}n$, where $\mathrm{d}\lambda$ is the peak position shift and $\mathrm{d}n$ is the refractive index difference.

CSRR structures ($p = 400$ nm and $l = 150$ nm) were coated with different materials, and their transmission properties were measured under 0° and 90° polarization, as shown in figure 4(a). We used water, alcohol and BSA to evaluate the CSRRs' detecting performance. The water and alcohol were used as they have different refractive indices of 1.33 and 1.36, respectively. They were filled into a slot on a PDMS plate, and then the CSRR sample was placed upside down on the slot. An obvious red-shift of the resonance peak was observed as shown in figure 4(b). According to the spectra of CSRRs coated with water and alcohol, the sensitivity is about 210 nm/RIU for 90° incidence, and 167 nm/RIU for 0° incidence. Compared with water and alcohol, BSA gives rise to a more obvious peak shift. The BSA was first dissolved in distilled water and a solution with a concentration of 15 μM was obtained, which was then dropped onto the CSRR structures and dried under room temperature. Measurements of the transmission showed that compared to uncoated CSRR structures the resonance peak shifted from 832 to 957 nm under 90° polarization, giving a net shift of 125 nm. This shows the possibility of plasmonic sensing by complementary MMs in the visible region. Moreover, such a complementary structure with a continuous layer of metal is convenient for the application of an external electric field to achieve active control, in which dynamic control of the spectrum may have specific sensitivity to biomolecules [20].

5. Conclusion

In conclusion, we have fabricated optical subwavelength CSRR structures with a minimum unit length of 100 nm and line width of 30 nm on gold films. The measured transmission spectra indicated that these nanoscale CSRR structures show noticeable anisotropic optical responses in the visible waveband from 600 to 900 nm under differently polarized incident light, and these transmission responses can be tuned by CSRR structure's period, metal thickness and unit length. Taking the metal dispersion into account, we considered that both the SPP and WMs play an important role in the transmission responses, and the coupling effect of the SPP and WM determines the position of the transmission peak. The CSRR is also shown to be RI sensitive to the dielectric environment with a sensitivity of 210 nm/RIU. For biomolecule detection, the protein BSA gives a net shift of 125 nm. An understanding of the mechanism of the nanoscale CSRR could improve the design of optical metamaterials and hence give impetus to its application in plasmonic sensing devices.

Acknowledgments

This work was supported by the National Basic Research Program of China (Grant No. 2009CB930502), the National Natural Science Foundation of China (Grants Nos 61001045, 91023041, 50825206, 10834012 and 11174362), and the Knowledge Innovation Project of CAS (Grant No. KJCX2-EW-W02). The authors also thank Professor Hongqiang Li at the Department of Physics at Fudan University for the advice and assistance.

References

[1] Raschke G, Kowarik S, Franzl T, Sönnichsen C, Klar T A, Feldmann J, Nichtl A and Kürzinger K 2003 *Nano Lett.* **3** 935–8

[2] Tan Y N, Su X, Zhu Y and Lee J Y 2010 *ACS Nano* **4** 5101–10

[3] Liu N, Tang M L, Hentschel M, Giessen H and Alivisatos A P 2011 *Nature Mater.* **10** 631–6

[4] Tao H *et al* 2011 *Adv. Mater.* **23** 3179–201

[5] Liedberg B, Nylander C and Lunström I 1983 *Sensors Actuators* **4** 299–304

[6] Ritchie R H, Arakawa E T, Cowan J J and Hamm R N 1968 *Phys. Rev. Lett.* **21** 1530–3

[7] Ghaemi H F, Thio T, Grupp D E, Ebbesen T W and Lezec H J 1998 *Phys. Rev.* B **58** 6779–82

[8] Kretschm E and Raether H 1968 *Z. Nat.forsch.* A **23** 2135

[9] Chiam S Y, Singh R, Zhang W and Bettiol A A 2010 *Appl. Phys. Lett.* **97** 191906

[10] He X J, Qiu L, Wang Y, Geng Z X, Wang J M and Gui T L 2011 *J. Infrared Millim. Waves* **32** 902–13

[11] Pryce I M, Kelaita Y A, Aydin K and Atwater H A 2011 *ACS Nano* **5** 8167–74

[12] Xu X L, Peng B, Li D H, Zhang J, Wong L M, Zhang Q, Wang S J and Xiong Q H 2011 *Nano Lett.* **11** 3232–8

[13] Falcone F, Lopetegi T, Laso M A G, Baena J D, Bonache J, Beruete M, Marqués R, Martín F and Sorolla M 2004 *Phys. Rev. Lett.* **93** 197401

[14] Khardikov V V, Iarko E O and Prosvirnin S L 2010 *J. Opt.* **12** 045102

[15] Bonache J *et al* 2005 *Microw. Opt. Technol. Lett.* **46** 508–12

[16] Bonache J, Gil I, García-García J and Martín F 2006 *IEEE Trans. Microw. Theory Tech.* **54** 265–71

[17] Kumar G, Cui A, Pandey S and Nahata A 2011 *Opt. Express* **19** 1072–80

[18] Vélez A, Sisó G, Campo A, Durán-Sindreu M, Bonache J and Martín F 2011 *Appl. Phys.* A **103** 911–4

[19] Zentgraf T, Meyrath T P, Seidel A, Kaiser S, Giessen H, Rockstuhl C and Lederer F 2007 *Phys. Rev.* B **76** 033407

[20] Sriram S, Bhaskaran M, Chen S, Jayawardhana S, Stoddart P R, Liu J Z, Medhekar N V, Kalantar-Zadeh K and Mitchell A 2012 *J. Am. Chem. Soc.* **134** 4646–53

[21] Oskooi A F, Roundy D, Ibanescu M, Bermel P, Joannopoulos J D and Johnson S G 2010 *Comput. Phys. Commun.* **181** 687–702

[22] Cai W and Shalaev V 2010 *Optical Metamaterials Fundamentals and Applications* (New York: Springer)

[23] Maier S A 2007 *Plasmonics: Fundamentals and Applications* (New York: Springer)

[24] Mary A, Rodrigo S G, Martín-Moreno L and García-Vidal F J 2007 *Phys. Rev.* B **76** 195414

[25] Gordon R and Brolo A G 2005 *Opt. Express* **13** 1933–8

[26] Suckling J R, Hibbins A P, Sambles J R and Lawrence C R 2005 *New J. Phys.* **7** 250